

PAPER • OPEN ACCESS

Static and modal analysis of sine-wave-shaped spar

To cite this article: E Elshazly *et al* 2021 *IOP Conf. Ser.: Mater. Sci. Eng.* **1172** 012002

View the [article online](#) for updates and enhancements.



ECS **240th ECS Meeting**
Digital Meeting, Oct 10-14, 2021
We are going fully digital!
Attendees register for free!
REGISTER NOW

Static and modal analysis of sine-wave-shaped spar

E Elshazly¹, M Kassem¹, M A Elshafei¹, and M Kamel¹

¹Department of Aircraft Mechanics, Military Technical College, EGYPT

E-mail: m_kassem@mtc.edu.eg

Abstract. Sine-Wave-shaped Spar (SWS) is recently involved in wing design as one of the corrugated shaped spars that highly improve the torsion and buckling resistance. SWS is an I-beam made of sine wave shaped vertical web fixed to upper and lower flanges. The current research evaluates the behavior of SWS in comparison to the traditional straight-web spar in resisting two cases of loading; static bending loading and static torsion loading. For each case, deformation and stress are analyzed. Modal analysis is also performed for the two spar configurations. For this purpose, a finite element model is developed using Ansys Workbench software for the SWS and the straight web spar. To reach a fair comparison, similar weight is considered for the two spar structures. A parametric study is performed to investigate the effect of web thickness and flange thickness on the bending and torsion deformation and stresses. The effect of thickness variation on the natural frequencies and mode shapes is also considered. The current study can be considered a base to design wing spars that combine the merits of the two spar configurations.

1. Introduction

The spar is the principal structural element of the wing that supports an aircraft during take-off, cruise and landing. In fact, spar design tends to have several interferences with the aircraft structural design. Nowadays, the strength and weight of the spar has become an important factor. Efforts are being made to reduce the weight of the aircraft and consequently increase the payload. The spars may be made of metal, wood or composite materials depending on the design criteria of a specific aircraft. They are generally classified into four different types by their cross-sectional configuration; solid, partly hollows, formed an I-beam and box shaped. Conventionally, the spar web is made of a vertical straight plate. However, introducing a sine wave shaped webs has attracted many researchers at various applications.

R. N. Hadcock [1] introduced the advanced composite materials to produce the sine wave spars of the horizontal stabilizer torque box of the military aircraft F-14A for the lightweight and the safety of the aircraft structures. To improve the cost, weight and integrity of the Northrop F-5E Fighter, it included sine wave spars and sine wave ribs [2]. Robert. K. Perrons [3] discussed the details of involving the development and production of the sine wave spars for the wings of F-22 by the Boeing Defense and Space Group, as sine wave provides the spar with a higher degree of mechanical stiffness.

Ren Yiru et al. [4] integrated a design concept for Boeing 737-200 aircraft to improve the crashworthiness of the fuselage using sine-wave beam and strut to dissipate impact kinetic energy by energy absorption structure during impact process. Sine wave composite spars were used in the main wing box of AV-8B/G R Mk5 Harrier II airframe, with four composite ribs made of sine wave construction [5].

S. Hanagud et al. [6] analyzed the static energy absorption behavior of graphite epoxy composite corrugated sine wave webs loaded in axial compression where crashworthy design has become a standard feature of many vehicle design processes. Garyl Farley et al. [7] reported crushing characteristics of



composite tubes with "Near-Elliptical" Cross Sections and showed that the energy absorbing beam webs evaluated in these studies consisted of sine-wave and integrally stiffened webs.

Harun Bayraktar, et al. [8] used three dimensional woven composites in sine-wave beam application to increase strength, stiffness, and thermal conductivity compared to conventional 2D laminated composites. Hartmut Pasternak and Dina Hannebauer [9] designed welded girders with sinusoidal corrugated webs. The sinusoidal corrugated web has a better buckling performance than classic welded sections and even comparable trapezoidally-shaped web. Krzysztof et al. [10] introduced numerical investigations of the behavior of a sinusoidal web loaded in shear due to buckling in the period from the onset of buckling until failure. William Rendall Johnson et al. [11] manufactured a sine wave beam web without bunching and distortion of the fibers of the composite web material and has a lightweight relative to strength and stiffness. The current research analyzes the sine-wave-shaped web spar compared with the straight-web spar from where static bending and static torsion are applied while keeping a similar weight of spars. A finite element analysis is performed using Ansys Workbench software. Moreover, a parametric study is conducted to find the effect of web thickness and flange thickness variations on the static response and modal analysis.

2. Spar configurations and modelling

The considered configurations of spar structures are shown in Figure 1. The spar consists of one vertical web and two horizontal flanges. The main difference between the two spar configurations is the vertical web. As shown in Figure 1(a), the straight-web spar is considered as an I-beam and is denoted by 'I' all through the paper. The straight-web thickness, length and height are denoted by t_{wI} , b , and L_{wI} , respectively. The sine-web spar has a corrugated web in a sine-wave shape and is denoted by 's' all through the paper. The current research represents the sine-web as semi-circles connected in a zigzag pattern as shown in Figure 1(b). The sine-web thickness, length and height are denoted by t_{ws} , b , and L_{ws} , respectively. L_{ws} is the perimeter of the sine wave shaped web. The thicknesses of the upper and lower flanges are denoted by t_{fU} and t_{fL} , and the spar length is L for both spar configurations.

The static loading applied on the spar structure is calculated for a wing of span ($L=3m$), aspect ratio 6, length of chord ($c=0.5m$) and the area ($S=1.5m^2$). Schrenk method is used to calculate distributed pressure and torsion load.

$$S = L * c = 3 * 0.5 = 1.5m^2. \quad (1)$$

$$Lift = \frac{1}{2} \rho V^2 S C_l = \frac{1}{2} * 1.225 * 40^2 * 1.5 * 0.8 = 1176 N. \quad (2)$$

$$P = \frac{L}{S} = \frac{1176}{1.5} = 784 N/m^2. \quad (Distributed\ pressure) \quad (3)$$

$$T = L \left(\frac{c}{3} - \frac{c}{4} \right) = 1176 * \left(\frac{0.5}{3} - \frac{0.5}{4} \right) \quad (Torsion\ load) \quad (4)$$

$$= 1176 * 0.04166 = 4849000 N/m$$

In the current research, the considered dimensions for the configurations of straight-web spar and sine-web spar are: the height of web is $b=109$ mm, the length of the straight-web spar is $L_{wI}=3000$ mm, the length of the sine-web spar is $L_{ws}=4717$ mm as determined in equation (5). The radius of the sine-web is $r=34.5$ mm, the number of the half cycles of the sine waves is $n=43.5$, the width of flange is $a=70$ mm, the web thickness (t_w) varies according to the loading. The flange thicknesses (t_{fU}, t_{fL}) are respectively the upper and the lower flange thickness. In spar design, flange thicknesses may vary according to the loading, however for simplicity, the current research considers the upper and the lower flange thicknesses equal ($t_{fU}=t_{fL}=3$ mm), unless other dimensions are mentioned.

The circumference length of the sine-web spar:

$$L_{ws} = \pi r n = \pi * 34.5 * 43.5 = 4717 mm \quad (5)$$

To maintain the same weight of the two spar configurations, the web thickness of the straight-web spar is $t_{wI}=1$ mm, while for the sine-web spar $t_{ws}=0.63542$ mm, unless other dimensions are mentioned.

Ansys workbench software is applied to establish the finite element model. SHELL181 element is used as it is suitable for analyzing thin to moderately-thick shell structures. It is a four-node element with six degrees of freedom at each node. Mesh selectivity analysis is conducted to achieve the convergence of deformation and stress results. Element size (9 mm), with a total number of elements (12691), is applied in the current research.

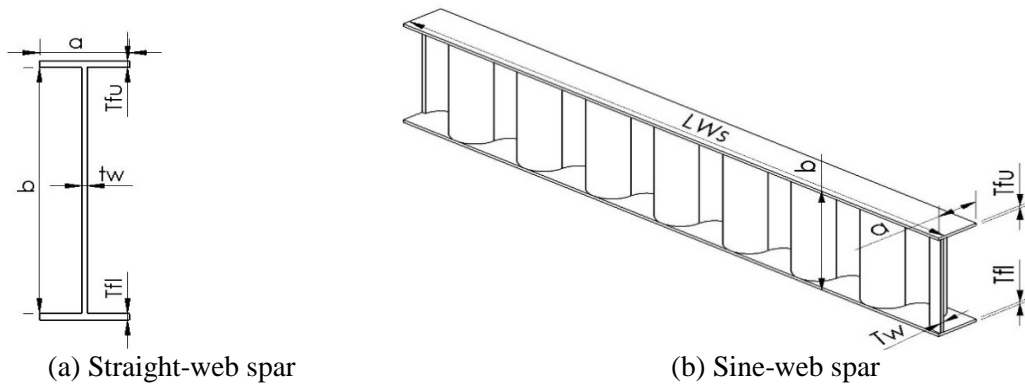


Figure 1. Configuration of spar structures

3. Static and modal analysis

3.1 Stress analysis due to static bending.

The distributed pressure is applied on the upper flange of the straight-web spar and the sine-web spar. The spars are fixed as a cantilever beam. The distributed pressure leads to bending deformation as shown in Figure 2 (a) and (b) for straight-web and sine-web spars, respectively. The bending stresses are shown in Figure 3 (a) and (b).

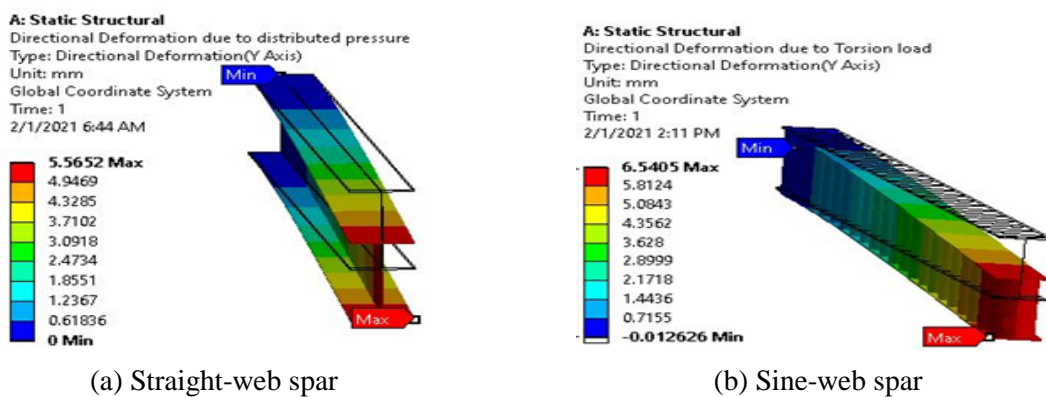


Figure 2. Static Bending deformation.

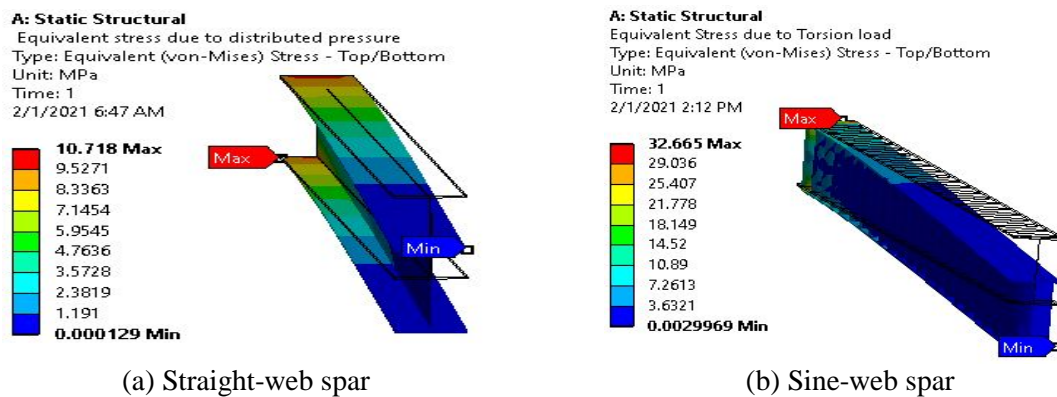


Figure 3. Static Bending stress.

3.2. Stress analysis due to static torsion.

The spars are fixed as a cantilever beam and the torsion load is applied at the free-end of spars. The torsion load on the I-beam spars leads to torsion deformation as shown in the Figure 4 (a) and (b) for straight-web and sine-web, respectively, and torsion stress as shown in the Figure 5 (a) and (b).

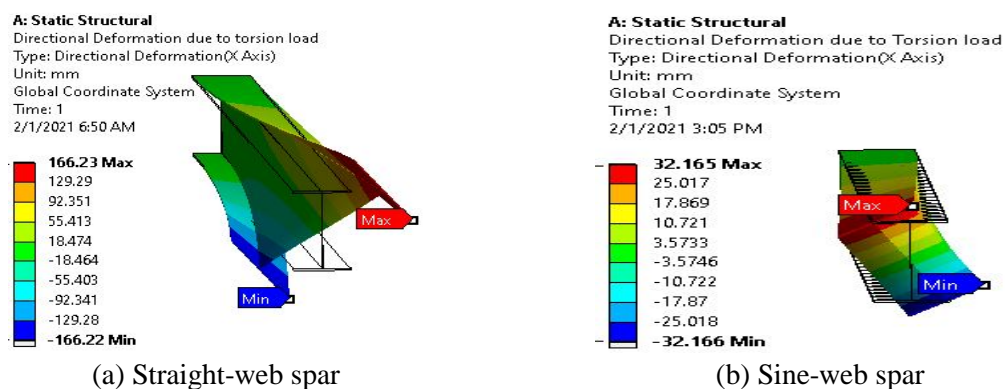


Figure 4. Static torsion deformation.

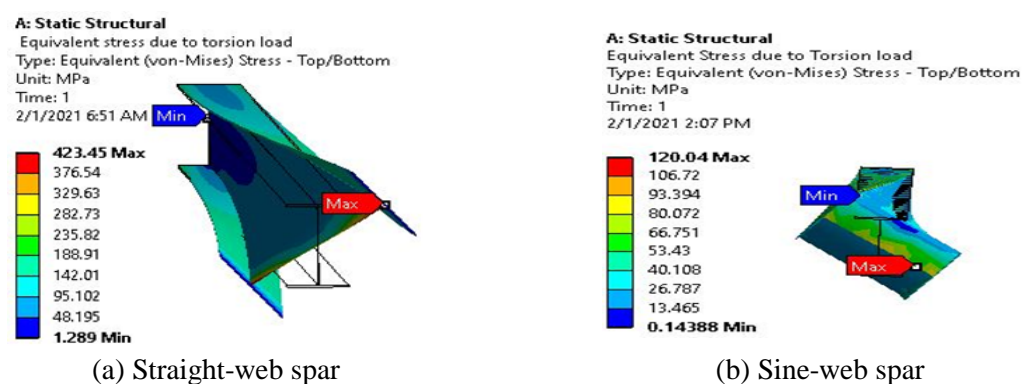


Figure 5. Static torsion stress.

3.3. Modal analysis.

The mode shapes of the straight-web and the sine-web spars describe the deformation that the spars would show when vibrating at the natural frequencies as shown in Figure 6 to Figure 9.

Figure 6 (a) shows the first mode shape of the straight-web spar, the first in-plane bending mode where $\omega_{11} = 5.6686 \text{ Hz}$. Figure 6 (b) shows the first mode shape of the sine-web spar, the first in-plane

bending mode where $\omega_{1S} = 5.731 \text{ Hz}$. There is a slight difference in the natural frequencies between the straight-web spar and the sine-web spar.

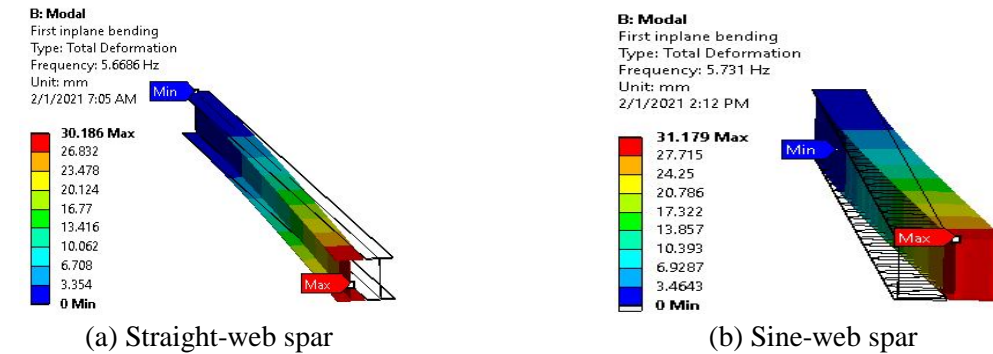


Figure 6. First in-plane bending mode.

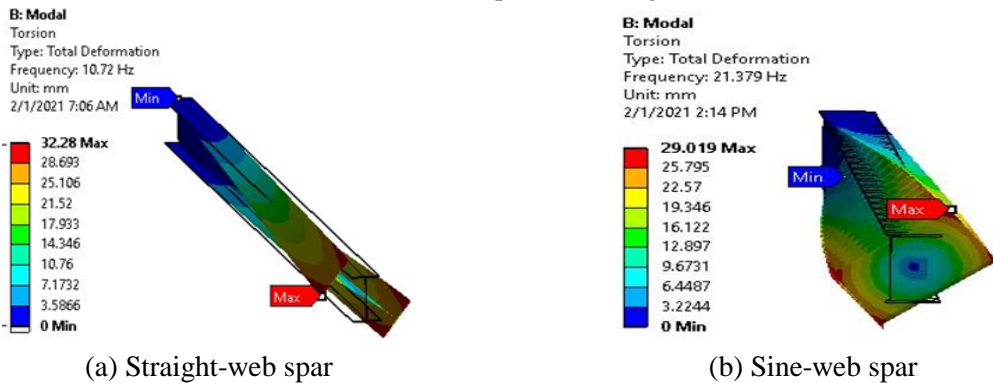


Figure 7. First torsion mode.

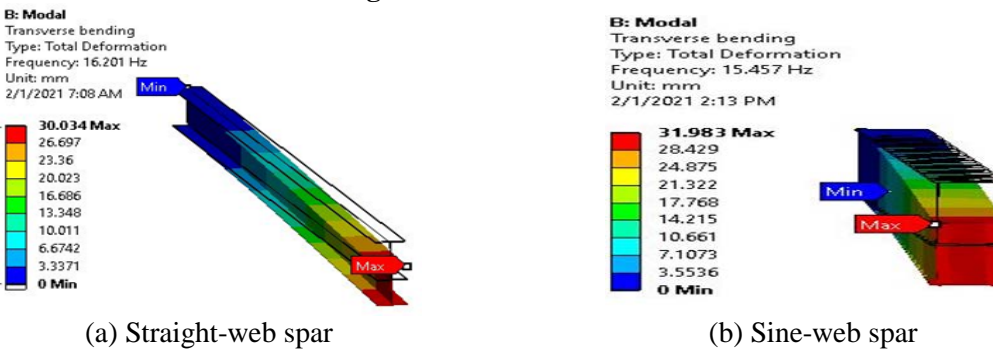


Figure 8. First transverse bending mode.

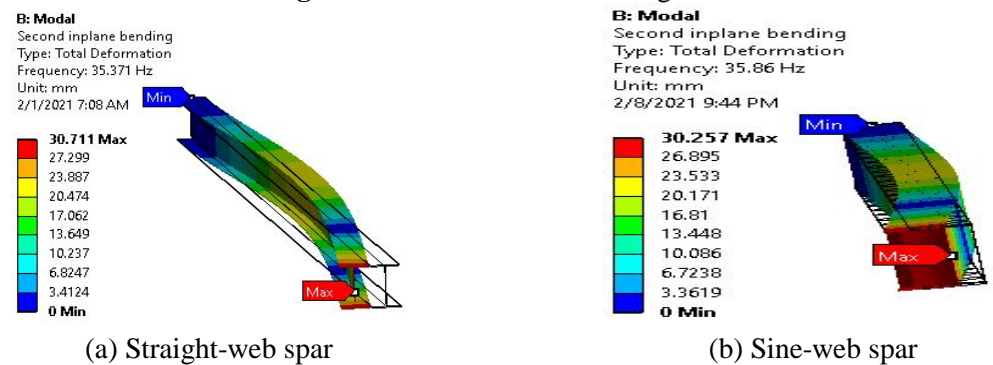


Figure 9. Second in-plane bending mode.

4. Parametric Study

4.1 Web thickness effect.

To obtain the influence of web thickness variation on the bending and torsional rigidity and the modal analysis, a parametric study is conducted. The straight-web thickness is varied from 1 mm to 10 mm. To obtain a fair comparison, the equivalent sine-web thickness is determined to maintain the same weight of the corresponding straight-web spar. Hence, the sine-web thickness is varied from 0.635 mm to 6.354 mm. It is worth mentioning that in all the plots of the current sub-section, the x-axis presents the straight-web thickness. The flange thickness is constant (3 mm) in the current subsection, while the following subsection investigates the effect of flange thickness variation.

Figure 10 shows the bending deformation due to a distributed pressure on the straight-web and the sine-web spars. The bending deformation decreases with increasing web thickness but the difference between the bending deformation of the straight-web and the sine-web spar increases starting at $\Delta w = 17.529\%$ up to $\Delta w = 75.832\%$, according to the relation $\Delta w = \frac{w_s - w_l}{w_l} \%$.

Figure 11 shows the bending stress due to a distributed pressure on the straight-web and the sine-web spars. Generally, the bending stress decreases with increasing web thickness, but the difference between the bending stress of the straight-web and the sine-web spar varies starting at $\Delta \sigma = 204.777\%$ down to $\Delta \sigma = 97.199\%$, according to the relation $\Delta \sigma = \frac{\sigma_s - \sigma_l}{\sigma_l} \%$.

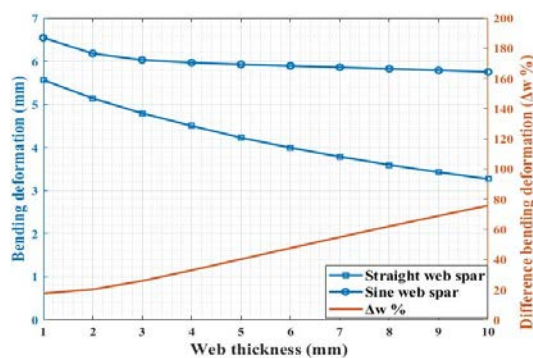


Figure 10. Bending deformation of straight and sine-web spar.

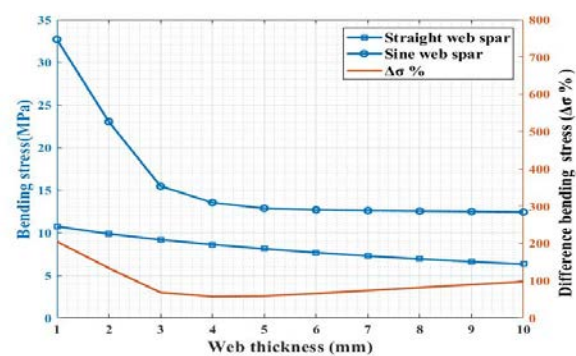


Figure 11. Bending stress of straight-web and sine-web spar.

Figure 12 and Figure 13 present the influence of web-thickness variation on the twist angle and the torsional stress, respectively, due to a static torsion on the free-end of the two spar configurations. As shown in Figure 12, the twist angle decreases with increasing the web thickness in both spar configurations. For small web thickness, the sine-web spar shows a torsional resistance greater than that of the straight-web spar, presented by a smaller twist angle. The difference of the twist angles starts at $\Delta \theta = -52.397\%$ at a straight web-thickness of 1 mm, then increases gradually to $\Delta \theta = 35.634\%$ at a straight-web thickness of 10 mm. The values of $\Delta \theta$ are determined according to the relation $\Delta \theta = \frac{\theta_s - \theta_l}{\theta_l} \%$.

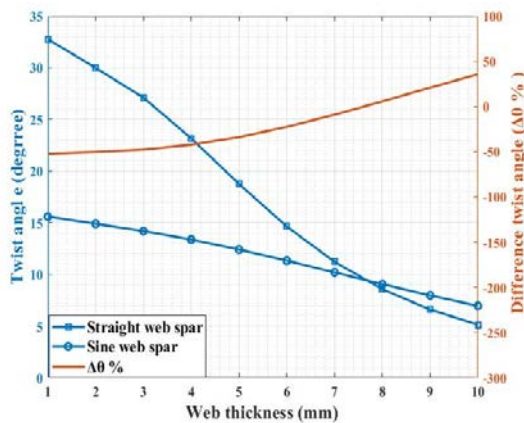


Figure 12. Twist angle due to torsion load on the straight-web and the sine-web.

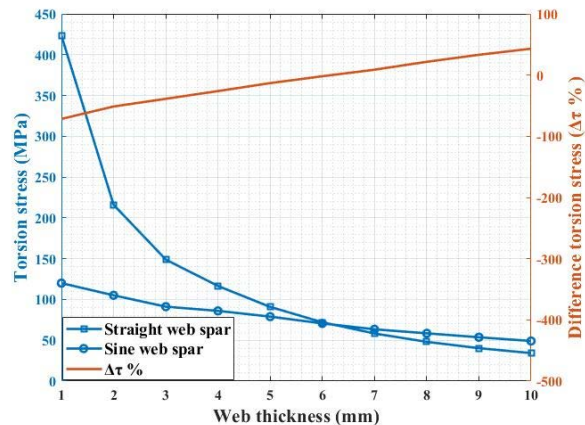
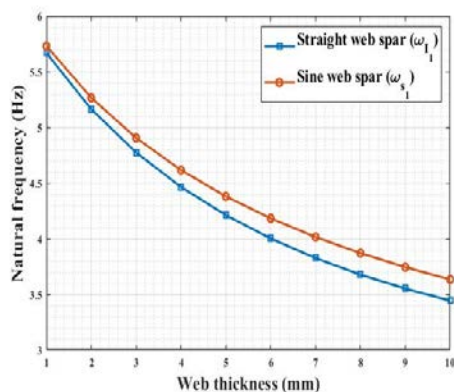


Figure 13. Torsion stress on the straight-web and the sine-web.

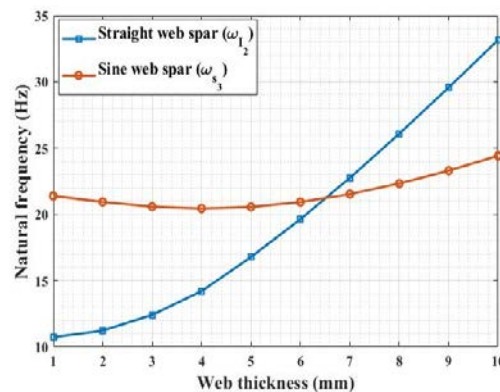
As shown in Figure 13, the torsion stress decreases with increasing web thickness but the difference of the torsion stress between the sine-web and the straight-web spars starts at $\Delta \tau = -71.652\%$ at a straight web-thickness of 1 mm then increases to $\Delta \tau = 43.119\%$ at a straight web-thickness of 10 mm. The values of $\Delta \tau$ are determined according to the relation $\Delta \tau = \frac{\tau_s - \tau_l}{\tau_l} \%$. Table 1 shows the results of the straight web spar and the sine web spar due to the distributed pressure and torsional load.

To compare the natural frequencies and mode shapes of the straight-web and sine-web spars of the same weight, the following parametric study is conducted by varying the web thickness. The results of the first four mode shapes are presented in Figure 14.

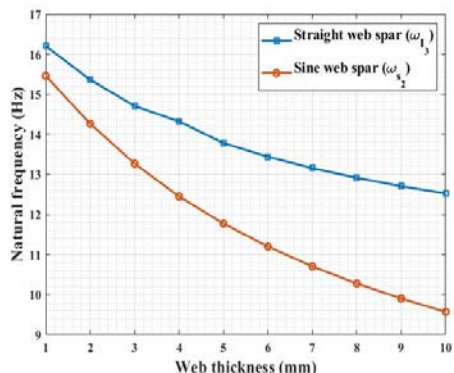
Figure 14 (a) shows the first mode shape of the straight-web and sine-web spars, the first in-plane bending mode. Generally, the first natural frequency of the sine-web spar is slightly greater than that of the straight-web spar. Figure 14 (b) shows the second mode shape of the straight-web spar, the first torsion mode and the third mode shape of the sine-web spar, the first torsion mode. Initially, the value of the first-torsion mode-shape of the sine-web spar is much greater than that of the straight-web spar at a straight-web thickness of 1 mm. Then, after a web-thickness of 6 mm, the value of the first-torsion mode-shape of the straight-web spar becomes greater. Figure 14 (c) shows the third mode shape of the straight-web spar, the first transverse bending mode and the second mode shape of the sine-web spar, the first transverse bending mode. Figure 14 (d) shows the fourth mode shape of the straight-web spar, the second in-plane bending mode and the fourth mode shape of the sine-web spar, the second in-plane bending mode, where there is a slight difference in the natural frequencies. Generally, the second in-plane bending mode natural frequency of the sine-web spar is slightly greater than that of the straight-web spar.



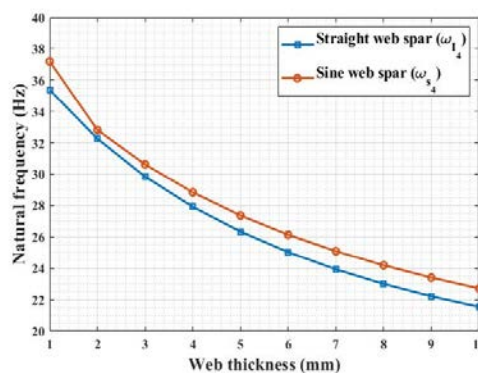
(a) First in-plane bending mode.



(b) First torsion mode.



(c) First transverse bending mode



(d) Second in-plane bending mode.

Figure 14. Mode shapes of straight and sine-web spars for variable web thickness (flange thickness is 3mm)

Table 1. Results of the straight web spar and the sine web spar due to the distributed pressure and torsional load.

Web thickness (mm)	Equivalent Web thickness (mm)	Distributed pressure				Torsion load			
		Straight web spar		Sine web spar		Straight web spar		Sine web spar	
		w_I (mm)	σ_I (MPa)	w_s (mm)	σ_s (MPa)	θ_I (deg.)	τ_I (MPa)	θ_s (deg.)	τ_s (MPa)
1	0.635	5.565	10.718	6.541	32.666	32.763	423.45	15.596	120.04
2	1.271	5.139	9.856	6.177	23.028	29.981	216.00	14.893	105.13
3	1.906	4.791	9.181	6.029	15.442	27.106	148.97	14.192	91.189
4	2.542	4.500	8.607	5.965	13.532	23.166	116.51	13.368	86.056
5	3.177	4.226	8.105	5.925	12.856	18.757	90.908	12.406	78.980
6	3.813	3.992	7.662	5.892	12.684	14.634	72.080	11.332	70.690
7	4.448	3.783	7.266	5.859	12.594	11.217	58.326	10.197	63.449
8	5.083	3.595	6.912	5.824	12.532	8.575	48.111	9.0581	58.544
9	5.719	3.425	6.589	5.788	12.476	6.598	40.349	7.9678	53.710
10	6.354	3.270	6.297	5.751	12.418	5.132	34.314	6.9605	49.110

4.2 Flange thickness effect.

A parametric study is conducted to investigate the effect of flange thickness variation on the static response and mode shapes of the straight-web and sine-web spars. The web thickness is maintained constant in the current sub-section. To keep the same weight of the two configurations, straight-web thickness is maintained at 1mm and the sine-web thickness is maintained at 0.63542 mm.

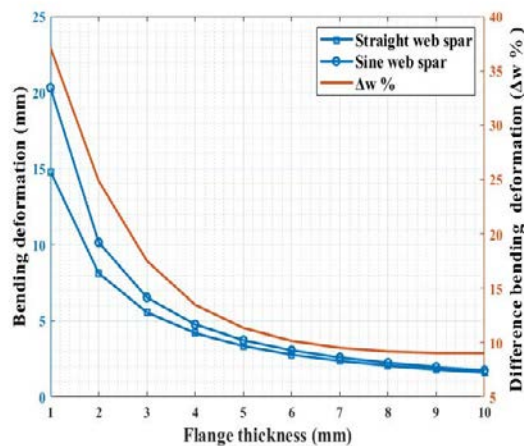


Figure 15. Bending deformation of straight and sine-web spars for variable flange thickness.

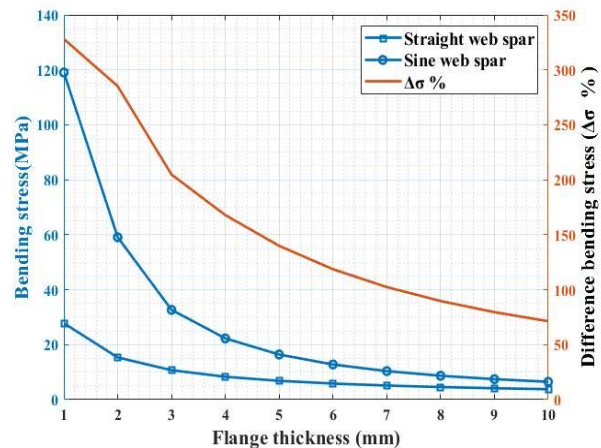


Figure 16. Bending stress on the straight-web and the sine-web for variable flange thickness.

Figure 15 shows the bending deformation due to distributed pressure on the straight-web and the sine-web spars at variable flange thicknesses. The bending deformation decreases with increasing the flange thickness but the difference between the bending deformation of the straight-web and the sine-web spar decreases starting at $\Delta w = 37.119\%$ down to $\Delta w = 9.041\%$. The values of Δw are obtained according to the relation $\Delta w = \frac{w_s - w_I}{w_I} \%$.

Figure 16 shows the bending stress due to distributed pressure on the straight-web and the sine-web spar at variable flange thicknesses. The bending stress decreases with increasing the flange thickness but the difference between the bending stress of the straight-web and the sine-web spar decreases starting at $\Delta \sigma = 328.01\%$ down to $\Delta \sigma = 71.345\%$. The values of $\Delta \sigma$ are obtained according to the relation $\Delta \sigma = \frac{\sigma_s - \sigma_I}{\sigma_I} \%$.

Figure 17 shows the twist angle due to torsion load on the straight-web and the sine-web spars at variable flange thicknesses. The twist angle decreases with increasing flange thickness but difference of the twist angle has a small value for the straight-web at $\Delta \theta = -5.320\%$ then this value decreases down to $\Delta \theta = -85.532\%$. The values of $\Delta \theta$ are obtained according to the relation $\Delta \theta = \frac{\theta_s - \theta_I}{\theta_I} \%$.

Figure 18 shows that the torsion stress decreases with increasing the flange thickness. The difference of the torsion stresses starts at $\Delta \tau = -41.303\%$ at a straight-web thickness of 1 mm, then this value decreases down to $\Delta \tau = -59.890\%$ at a straight-web thickness of 10 mm. The values of $\Delta \tau$ are obtained according to the relation $\Delta \tau = \frac{\tau_s - \tau_I}{\tau_I} \%$.

It is concluded that increasing flange thickness for the sine-web spar is better than the straight-web spar where the twist angle and the torsion stress due to the torsion load decrease with a higher rate than that of the straight-web spar.

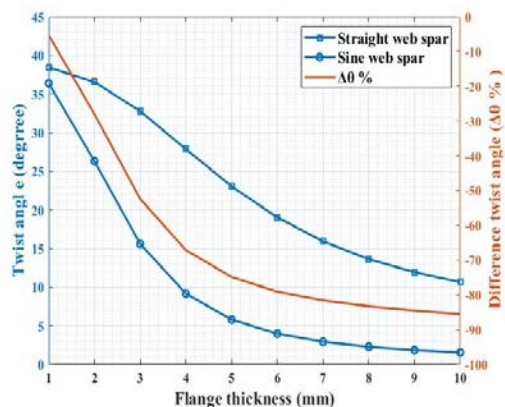


Figure 17. Twist angle due to torsion load on the straight-web and the sine-web for variable flange thickness.

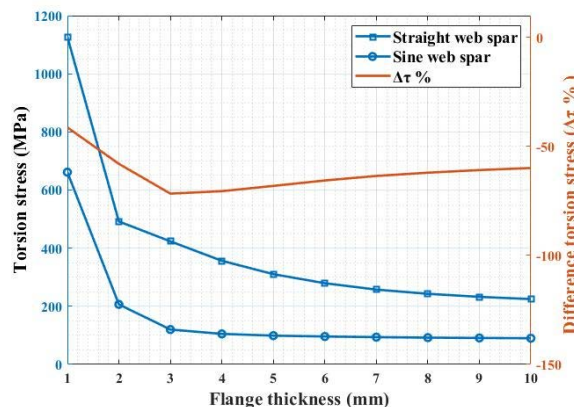
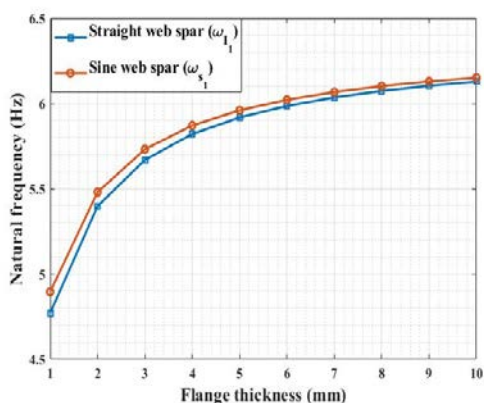
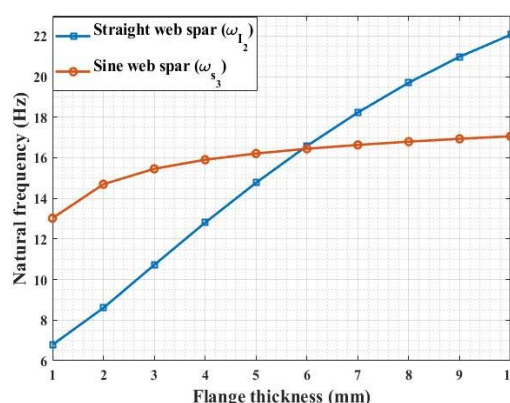


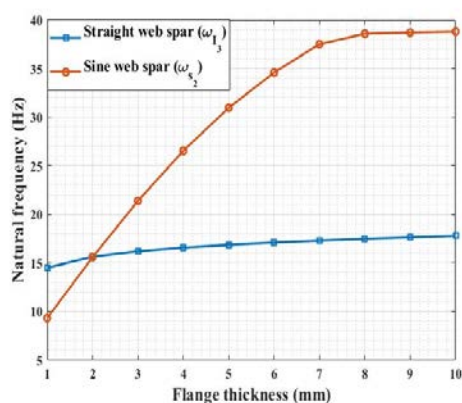
Figure 18. Torsion stress on the straight-web and the sine-web for variable flange thickness.



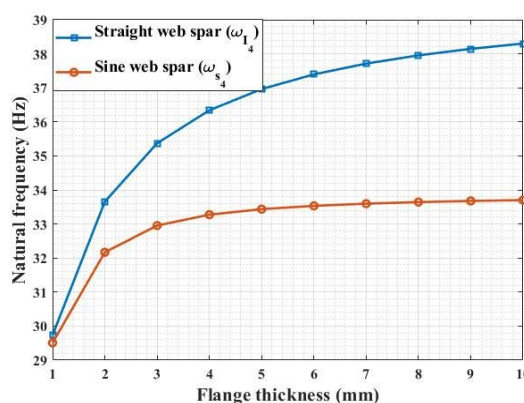
(a) First in-plane bending mode.



(b) First torsion mode.



(c) First transverse bending mode



(d) Second in-plane bending mode.

Figure 19. Mode shapes of straight and sine-web spars for variable flange thickness (straight-web thickness is 1mm and the sine-web thickness is 0.63542mm)

The natural frequencies of the first four mode-shapes are obtained for the straight-web and sine-web spar to analyze the influence of flange thickness variation. Figure 19 (a) shows the first mode shape of the straight-web and the sine-web spars, the first in-plane bending mode, where there is a slight difference in the natural frequencies. Figure 19 (b) shows the second mode shape of the straight-web spar and the third mode shape of the sine-web spar, the first torsion mode. Figure 19 (c) shows the third mode shape of the straight-web spar and the second mode shape of the sine-web spar, the first transverse bending mode. Figure

19 (d) shows the fourth mode shape of the straight-web spar and the fourth mode shape of the sine-web spar, the second in-plane bending mode.

From the parametric study, it is concluded that varying the web thickness and the flange thickness greatly affects the static and dynamic performance of both straight-web and sine-web spar structures. Consequently, it is advisable to optimize the spar dimensions and configuration according to loading condition and application.

5. Conclusion

Static and modal analyses of sine-web spar are conducted and compared to the straight-web spar. To achieve a fair comparison, the sine-web thickness is selected to maintain the same weight of both configurations. Results show that although sine-web spar loses bending rigidity compared to the straight-web spar, it affords torsional resistance that exceeds that of the straight-web spar. It also retards the torsion mode by increasing its natural frequency. A parametric study is performed to investigate the effect of both web thickness and flange thickness variation on the static response and natural frequencies of the spar configurations. It is concluded that increasing the web thickness, while keeping the same weight of spars, increases the bending rigidity of the straight spar with a rate higher than that of the sine-web spar. It is clear that the web thickness needs to be optimized to obtain the optimum performance while keeping the weight as minimum as possible. This shows promising results to obtain an optimized spar structure that combines the merits of both spar configurations.

References

- [1] Hadcok R 1977 The applications of advanced composites to military aircraft. I. p. 10.
- [2] Figge F A and Bernhardt L 1975 Air superiority fighter wing structure design for improved cost, weight, and integrity. *Journal of Aircraft*, 12(8), pp.670-675.
- [3] Perrons R K 1997 Make-buy decisions in the U.S aircraft industry,p.144.
- [4] Ren Yiru X J 2016 Crashworthiness analysis of aircraft fuselage with sine-wave beam structure.*Chinese Journal of Aeronautics*, p. 8.
- [5] Riley B L 1986 AV-SB/GR Mk 5 airframe composite applications. *MechE*, vol. 200, p. 17.
- [6] Hanagud J I 1989 Energy absorption behavior of graphite epoxy composite sine webs. *Journal of composite materials*, vol. 23, p. 12.
- [7] Gary R and Farley L 1992 Crushing characteristics of composite tubes with "near-elliptical" cross sections .*Technomic Publishing Co.,Inc.*, p. 11.
- [8] Bayraktar I 2012 Development of realistic simulation techniques to predict cure -induced microcracking in 3d woven composites.
- [9] Pasternak D H Beams and Columns with sinusoidal corrugated webs. p. 8.
- [10] Krzysztof S 2020 Finite element analysis of the stability of a sinusoidal web in steel and composite steel-concrete girders, p. 15.
- [11] Johnson R R W 1978 Sine wave beam web and method of manufacture,united states patent 818,910.
- [12] Jenkis J M 1979 Criteria for representing circular arc and sine wave spar webs by non-curved elements, national technical information service, p. 15